JAAS
Journal of Analytical Atomic Spectrometry

Computer Simulation of an Analytical Direct Current Glow Discharge in Argon: Influence of the Cell Dimensions on the Plasma Quantities

ANNEMIE BOGAERTS* AND RENAAT GIJBELS

Department of Chemistry, University of Antwerp, Universiteitsplein 1, B-2610 Wilrijk-Antwerp, Belgium

A set of three-dimensional mathematical models was developed for describing the behavior of the different plasma species in a direct current glow discharge in argon used as an analytical ion source for mass spectrometry. The models were applied to cylindrical cells (flat cathode and hollow anode) with various dimensions to study the effect of the dimensions on the calculated plasma quantities. The results show that the cell dimensions have no significant influence on the qualitative behavior of the plasma quantities, but they do affect the absolute values, at least for cell dimensions ranging from 0.5 to 2 cm. For larger cells, the absolute values also remain more or less constant. The results suggest that, for the selected discharge conditions of 1000 V, 1 Torr and about 2 mA and a copper cathode, a cell with both length and radius equal to 2 cm is a good choice for analytical mass spectrometry. This paper demonstrates that the models are in principle able to predict trends in plasma behavior and performance in analytical applications and that they can therefore be useful in developing new cells.

Keywords: *Glow discharge; modeling; cell design*

Glow discharges are used for a range of applications: as spectroscopic sources for mass spectrometry or optical spectrometric techniques,[1] for deposition of thin films and for plasma etching and modification of surfaces in the semiconductor industry,[2] as plasma displays, as metal vapor ion lasers and also in the lighting industry. It is to be expected that the results in the different application fields will depend strongly on the cell configuration. One possibility for optimization is to build different cells and to investigate which configuration and which dimensions yield the best results. However, this is sometimes based on trial and error, and it can be a time-consuming and expensive approach. It would be much cheaper to predict the optimum cell configuration by computer simulations prior to building the cells.

We have developed a set of mathematical models for describing the behavior of the different species present in a direct current glow discharge in argon used as an ion source for mass spectrometry. These models were first developed in one dimension[3–8] and later extended to three dimensions and applied to the standard cell used for analyzing flat samples in a VG9000 glow discharge mass spectrometer.[9–12] Reasonable agreement with experimental results (*e.g.*, based on laser-induced atomic fluorescence measurements) could be achieved.[13–15] These models can in principle be used to predict the optimum cell design.[16] To illustrate this in the present paper, the models were applied to a simple, cylindrically symmetrical glow discharge cell with a flat cathode. The cell configuration was kept constant, but the length and the radius of the cell were varied to investigate their influence on the calculated quantities.

DESCRIPTION OF THE MODELS

A number of separate models have been developed for the different plasma species in a direct current glow discharge in argon with a copper cathode, and these models were combined to obtain an overall picture of the glow discharge. Table 1 gives an overview of the different species assumed to be present in the plasma and the models used to describe these species. Fluid models are utilized for plasma species that are more or less in equilibrium with the electric field in the discharge (*i.e.,* the energy gained by the electric field is more or less balanced by the energy lost due to collisions), so that they can be considered as a fluid and described with continuity and transport equations. Monte Carlo simulations are employed for plasma species that are far from equilibrium, so that their behavior has to be described explicitly (*i.e.,* trajectory calculated with Newton's laws and collisions treated statistically by random numbers). A short explanation of the different models (*i.e.,* the relevant processes considered in each model) is also included in Table 1. The models are combined and solved iteratively until final convergence is reached. More information about these models can be found elsewhere.[3–12]

The models are applied to the cell geometry represented in Fig. 1. We chose a very simple and general cell configuration, so that the results of this study can most easily be applied to various, more specific types of cell geometries. The length and radius of the cell are each varied independently between 0.5 and 4 cm. In the initial 'standard cell', the length and radius are each taken as 2 cm. A metallic disk of 0.25 cm radius acts as the cathode and is represented by the black rectangle at $l = 0$. All the other cell walls (*i.e.,* the cylindrical portion and the cylinder ends) are at anode potential. The cathode and anode are separated by an insulating ring (0.1 cm wide). The fluid models are developed in two dimensions: due to the cylindrical symmetry of the cell, the three dimensions could, indeed, be reduced to two dimensions. The Monte Carlo models, however, are completely constructed in three dimensions.

RESULTS AND DISCUSSION

Discharge Current as a Function of Voltage and Pressure

The calculations were all performed at a 1000 V discharge voltage and 1 Torr argon gas pressure. When the pressure, voltage and gas temperature are given, the models allow the self-consistent calculation of the electrical current flowing through the cell. Comparison of the calculated currents with experimental values can then be used to test whether the models present a realistic picture of the glow discharge. Assuming a gas temperature of 450 K, the calculated currents for the different cell dimensions investigated are presented in Table 2. They range from 0.7 to 2.6 mA for all cell dimensions under study. Hence the discharge conditions investigated (1000 V, 1 Torr and 0.7–2.6 mA) are typical discharge conditions for glow discharge mass spectrometry (GDMS).

Table 1 Overview of the plasma species assumed to be present in the glow discharge plasma, the models used to describe these species, the relevant processes considered in these models and references giving more information about these models

Plasma species	Model	Relevant processes	Ref.
Ar atoms at rest	Not explicitly calculated	Atoms assumed to be uniformly distributed throughout the cell	—
Fast electrons (*i.e.* energy high enough for inelastic collisions)	Monte Carlo model	Elastic collisions with Ar atoms; electron impact ionization of Ar atoms in the ground state and in the metastable level, and of sputtered Cu atoms; electron impact excitation of Ar atoms in the ground and metastable states	3,4,9
Thermalized electrons	Fluid model	Continuity and transport equations (transport by diffusion and migration in the electric field); equations coupled to Poisson equation, to obtain self-consistent electric field	4,9
Ar^+ ions	Fluid model	idem	4,9
Ar^+ ions in the CDS*	Monte Carlo model	Symmetric charge transfer; elastic collisions with Ar atoms; ion impact ionization and excitation of Ar atoms	3,5,9
Ar fast atoms in the CDS	Monte Carlo model	Elastic collisions with Ar atoms; atom impact ionization and excitation of Ar atoms	3,5,9
Ar metastable atoms	Fluid model	Balance equation with different production terms (electron, ion and atom impact excitation to the metastable levels and electron–ion radiative recombination), and loss terms (electron impact ionization and excitation from the metastable levels, electron collisional transfer to the nearby levels, metastable atom–metastable atom collisions, Penning ionization of sputtered Cu atoms, two- and three-body collisions with Ar atoms); moreover, transport is diffusion controlled, and subsequent de-excitation at the walls is an additional loss process	6,11
Cu atoms	Monte Carlo model	Thermalization immediately after sputtering, due to collisions with Ar gas atoms	10
Cu atoms and Cu^+ ions	Fluid model	Further transport of Cu atoms (diffusion controlled), ionization of Cu atoms (by Penning ionization by Ar metastable atoms, asymmetric charge transfer by Ar ions and electron impact ionization) and transport of the Cu ions (by diffusion and migration in the electric field)	7,11
Cu^+ ions in the CDS	Monte Carlo model	Elastic collisions with Ar atoms	7,11

* CDS = Cathode Dark Space.

Table 2 Calculated quantities for the different cell dimensions investigated (at 1000 V and 1 Torr, argon discharge with copper cathode)

Parameter	$l=2$ cm $r=2$ cm	$l=0.5$ cm $r=2$ cm	$l=1$ cm $r=2$ cm	$l=3$ cm $r=2$ cm	$l=4$ cm $r=2$ cm	$l=2$ cm $r=0.5$ cm	$l=2$ cm $r=1$ cm	$l=2$ cm $r=3$ cm	$l=2$ cm $r=4$ cm
Electric current/mA	2.4	0.65	1.9	2.45	2.5	0.87	1.3	2.5	2.55
Length of the CDS/cm	0.15	0.23	0.16	0.15	0.145	0.20	0.17	0.15	0.15
Max. value of the plasma potential/V	1.9	4.6	2.2	1.9	1.9	9.8	3.8	1.9	1.9
Max. axial electric field strength at cathode/kV cm^{-1}	−20	−15	−19	−20	−20	−15	−17	−20	−20
Max. axial electric field strength at anode end-plate/V cm^{-1}	13	240	36	7	4	70	27	12	12
Max. radial electric field strength at anode side-walls/V cm^{-1}	5	2	3	5	4.5	413	32	1.6	0.8
Max. value of Ar ion and thermalized electron density/cm^{-3}	1.9×10^{12}	1.6×10^{11}	1.3×10^{12}	1.9×10^{12}	2.0×10^{12}	5.7×10^{11}	8.4×10^{11}	2.0×10^{12}	2.1×10^{12}
Max. value of fast electron density/cm^{-3}	9.6×10^{7}	3.4×10^{7}	8.7×10^{7}	9.9×10^{7}	1.1×10^{8}	5.7×10^{7}	5.8×10^{7}	9.9×10^{7}	9.9×10^{7}
Max. value of sputtered Cu atom density/cm^{-3}	2.1×10^{13}	4.6×10^{12}	1.7×10^{13}	2.1×10^{13}	2.1×10^{13}	2.0×10^{12}	3.5×10^{12}	2.1×10^{13}	2.1×10^{13}
Max. value of Cu ion density/cm^{-3}	4.6×10^{10}	2.5×10^{8}	1.8×10^{10}	4.7×10^{10}	5.5×10^{10}	1.4×10^{9}	4.1×10^{9}	5.7×10^{10}	5.9×10^{10}
Ratio of Cu ion to Ar ion density (%)	2.4	0.16	1.4	2.5	2.8	0.25	0.50	2.9	2.8
Degree of ionization of Cu (%)	2.1	0.009	0.57	2.4	2.7	0.033	0.23	4.1	4.2

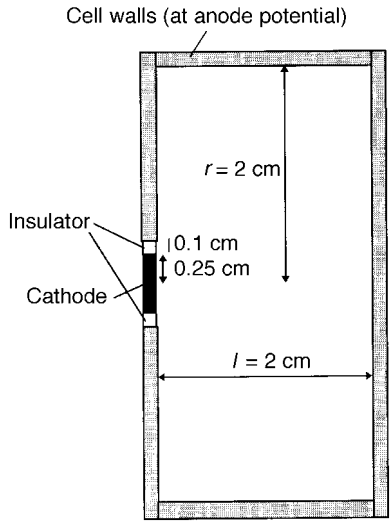

Fig. 1 Schematic diagram of the cylindrical glow discharge cell with various dimensions to which the models were applied (flat cathode and hollow anode). The cell with length (l) and radius (r) equal to 2 cm is taken as the 'standard cell'. The lengths and radii were each varied independently from 0.5 cm to 4 cm.

It appears that for lengths and radii smaller than 2 cm, the current increases clearly with increasing length and radius. The fast electrons can travel longer in the plasma before they reach the walls and can hence give rise to more ionization collisions, more electron multiplication and hence higher currents. Moreover, the ions and (slow) electrons will not arrive so rapidly at the walls, where they would be neutralized by electron–ion recombination, so that their density in the plasma is higher and they can carry more current. At lengths and radii larger than 2 cm, the calculated current does not appear to increase further. This indicates that at the selected discharge conditions the range in which fast electrons can produce ionization collisions is more or less limited to about 2 cm from the cathode (see below).

Potential and Electric Field Distributions

Fig. 2 presents the potential distribution throughout the discharge for the cell of length and radius 2 cm. The cathode is represented by the black rectangle at $z=0$. The potential is -1000 V at the cathode, and increases rapidly immediately in front of the cathode. It goes through zero at about 0.15 cm from the cathode, and is slightly positive (about 1.9 V, the plasma potential) in the rest of the plasma. The position where the potential goes through zero defines the interface between Cathode Dark Space (CDS) and negative glow (NG), and it is therefore indicated with a thicker line. The potential distributions calculated for the other cell dimensions are qualitatively the same. The length of the CDS is always more or less similar, as can be seen from Table 2, except at the smallest lengths and radii investigated, since the current is lower there; hence the electrons cannot give rise to so much ionization, and the CDS therefore has to be longer to sustain the discharge. The NG always fills up the rest of the discharge cell, thus being small for the small dimensions and large for the larger dimensions. The value of the plasma potential was calculated to be roughly constant for lengths and radii $\geqslant 2$ cm, but increased for shorter lengths and radii (see Table 2). The reason for this is found in the phenomenon of 'sheath formation' (Debye shielding):[2] if the potential in the plasma is perturbed, the plasma reacts to oppose that change. Since the electrons have a much higher mobility than the argon ions, they will diffuse more rapidly to the walls, where they will be lost, and

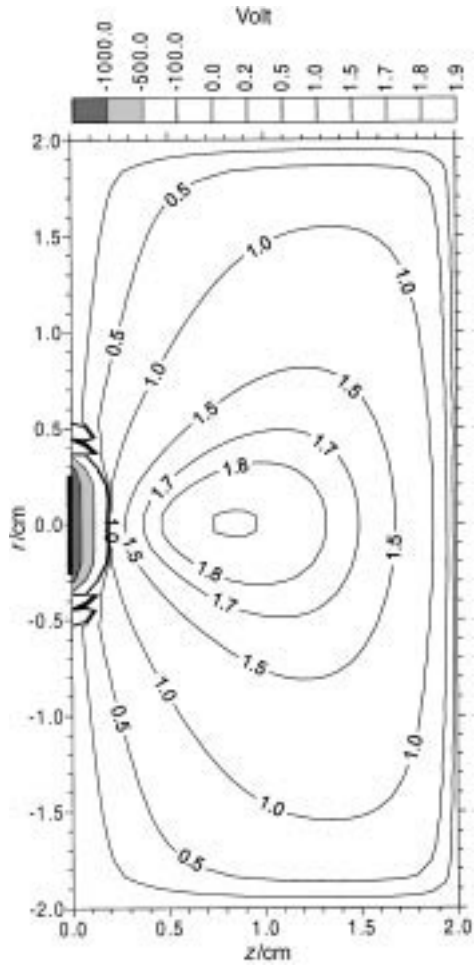

Fig. 2 Calculated potential distribution for the standard cell ($l=r=$ 2 cm) at 1000 V, 1 Torr and 2.4 mA in an argon discharge with copper cathode.

the thin plasma sheath in front of the walls stays behind with a positive space charge. This leads to a potential increase in the plasma with respect to the walls, which gives rise to a positive plasma potential, *i.e.,* the plasma is the most positive body in the discharge. It can be understood that in a small discharge cell, the perturbation by the walls is more significant, and the plasma has to react more to oppose the potential change at the walls, yielding a higher (more positive) plasma potential. The position where the plasma potential reaches its maximum is slightly closer than about 1 cm from the cathode for the cells with lengths and radii $\geqslant 2$ cm (hence it is not always in the middle of the discharge cell, as one might expect), and it was found to be at about 0.4–0.5 cm from the cathode for the cells with smaller dimensions. The cell dimensions investigated here do not yet appear to be large enough to give rise to the formation of a Faraday dark space or positive column, although when $l=2$ cm and $r=4$ cm the calculated potential again becomes slightly negative (about -0.2 V) at a radial position of about 3 cm from the cell axis, which indicates the beginning of a Faraday dark space being formed.

From the potential distributions, the electric field strengths throughout the discharge can also be calculated. The axial electric field is extremely negative at the cathode (due to a large potential drop over a small distance), it increases rapidly in the CDS to small negative values at the interface with the NG, it crosses the zero-line always at about 0.5–1.2 cm from the cathode (called 'field-reversal;' it occurs at the position where the potential reaches its maximum) and it increases to small positive values at the anode end-wall. The radial electric

field is negative in the CDS at the edges of the cathode and it is slightly positive in the NG, increasing slightly towards the anode side-walls. These electric field distributions are qualitatively similar to those calculated for the VG9000 glow discharge cell,[9] and are therefore not illustrated here again. Table 2 presents the maximum values of the axial electric field strengths at the cathode and at the anode end-wall, and the maximum values of the radial electric field strengths at the anode side-walls for the different cell dimensions investigated. It appears that the axial electric field at the cathode increases for lengths and radii increasing from 0.5 to 2 cm (because the CDS becomes shorter and the potential has to fall over a shorter distance, giving rise to a higher electric field), and is approximately constant for the larger dimensions (because the CDS length was also found to be more or less constant). The axial electric field at the anode end-wall increases considerably for decreasing cell lengths, which is attributed to the shorter distance over which the potential has to drop to zero at the wall. The effect is most pronounced for the small values of l, since these are also characterized by a higher plasma potential that has to drop off. The effect of the increasing radius is only small, since the length (and hence the distance over which the potential has to fall in the axial direction) stays constant. The higher axial electric field at the anode end-wall in the case of the small radii is due to the higher plasma potential, but for radii ranging from 2 to 4 cm the axial electric field is constant, since both the plasma potential and the axial distance are the same. On the other hand, the values of the radial electric fields at the anode side-walls change considerably for the different radii investigated, as can be seen from Table 2, because (i) the distance over which the plasma potential has to fall to zero varies widely and (ii) at small values of r, a higher plasma potential has to drop off. Also, on decreasing the lengths, the radial electric field at the anode side-walls increases, but the effect is only visible at small values of l, owing to the higher plasma potential that has to drop off to zero, and it is absent at $l \geqslant 2$ cm, since both the value of the plasma potential and the distance over which the potential has to fall stay constant.

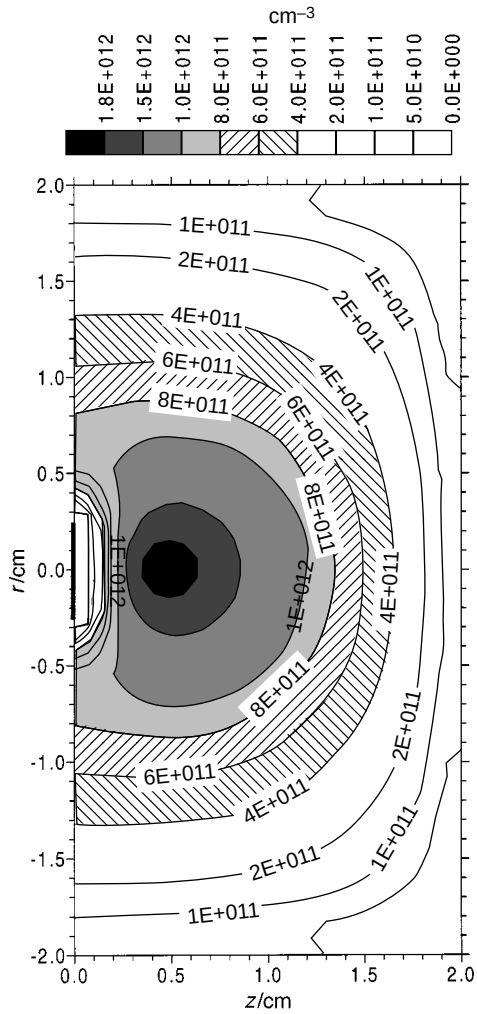

Fig. 3 Calculated density profile of the argon ions for the standard cell under the same discharge conditions as in Fig. 2.

Density of Argon Ions and Slow Electrons

In Fig. 3, the argon ion density distribution is illustrated for the cell with length and radius both equal to 2 cm. The argon ion density is low and more or less constant in the CDS, rises rapidly at the interface between CDS and NG and reaches its maximum at about 0.5 cm from the cathode. It decreases again to low values at the cell walls. The slow electron density profile (not shown here) is almost identical, except that it is zero in the CDS and at the cell walls. This gives rise to a net positive space charge in the CDS and in the small sheaths adjacent to the other walls and to charge neutrality in the NG, and it defines therefore the typical potential distribution shown in Fig. 2. The maximum of the argon ion density lies closer to the cathode than the position of the maximum plasma potential, since the production of argon ions (*i.e.,* mainly by electron impact ionization) is also peaked closer to the cathode (see below). The argon ion density distributions calculated for the other cell dimensions are qualitatively the same: the density is low in the CDS and reaches its maximum in all cases at about 0.4–0.5 cm from the cathode. The density values at the maximum of the profiles are given in Table 2. They increase when the dimensions become larger, because the 'sink' at the walls (neutralization due to electron–ion recombination) becomes less important. The effect is most pronounced for lengths and radii between 0.5 and 2 cm, and is almost negligible for the larger dimensions. This shows that the sink effect of the walls only plays a role in the small discharge cells, and that for larger cells it makes no real contribution in determining the density in the plasma.

Density of Fast Electrons

Fig. 4 shows the fast electron density distribution for the cell with length and radius both equal to 2 cm. The density reaches its maximum at the interface between CDS and NG and decreases towards the walls. The electrons have the longest 'residence time' at the CDS–NG interface and in the beginning of the NG, owing to back and forth scattering. The fast electron density distributions calculated for the other cell dimensions are very similar to that in Fig. 4, *i.e.,* they reach also their maximum at the CDS–NG interface and decrease towards the walls. The values at the maxima for the different cell dimensions are given in Table 2. The fast electron density increases for lengths and radii ranging from 0.5 to 2 cm and remains constant for larger dimensions. In the small cells, the fast electrons can easily reach the walls, where they can be absorbed or reflected (probably with lower energies, *i.e.,* secondary electron emission). The walls therefore act either as a particle sink (in the case of electron absorption) or, which is more important, as an energy sink for the electrons (in the case of secondary electron emission; most of the fast electrons are 'converted' to slow electrons). In both cases, fast electrons are 'lost' at the walls. For the larger cells, the effect of the walls as a sink for the fast electron density is unimportant. It appears that the range of the fast electrons is about 2 cm under the present discharge conditions, hence for larger cells the electrons seem to be more or less thermalized before they can reach the walls.

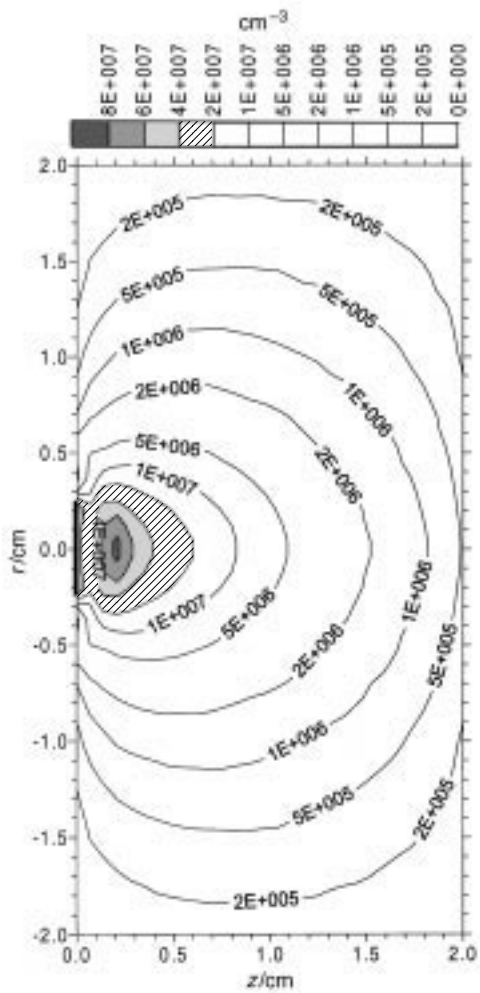

Fig. 4 Calculated density profile of the fast electrons for the standard cell under the same discharge conditions as in Fig. 2.

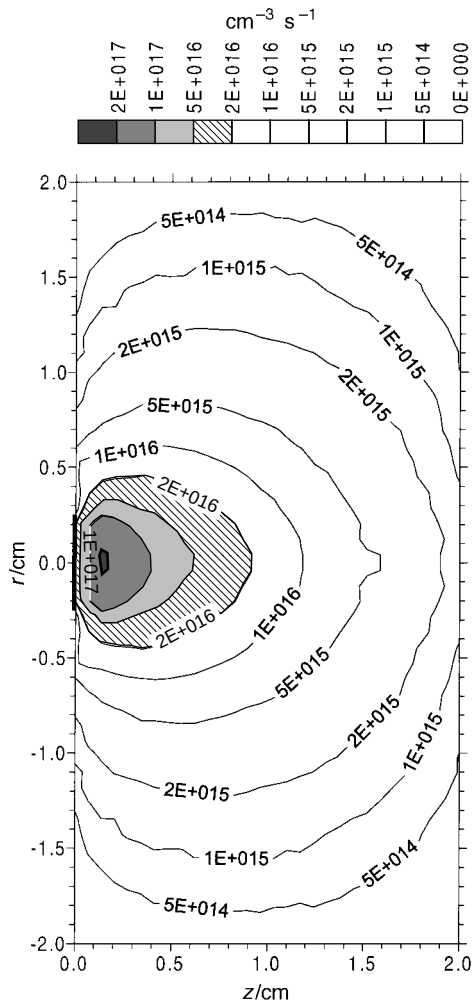

Fig. 5 Calculated electron impact ionization rate for the standard cell under the same discharge conditions as in Fig. 2.

Electron Impact Ionization Rate

The rate of discharge gas ionization, produced by the fast electrons, is depicted in Fig. 5. The shape of the electron impact ionization rate is similar to the fast electron density profile: a maximum is reached at the interface between CDS and NG, whereafter the rate decreases again towards the cell walls. The ionization rates calculated for the other cell dimensions are comparable, with a maximum at the CDS–NG interface and a decrease towards the walls. For the small cells (l or $r \leqslant 2$ cm), the maximum value is lower than the maximum in Fig. 5, since the fast electrons are lost more easily at the walls and cannot give rise to so much ionization. On the other hand, the larger cells (l or $r \geqslant 2$ cm) do not give rise to more ionization, *i.e.,* the maximum value is of comparable magnitude to that in Fig. 5, and the ionization rate further than 2 cm from the cathode is negligible. The range of electrons to produce ionization seems to be more or less restricted to within about 2 cm from the cathode. Therefore, it appears that for the present discharge conditions a cell with both length and radius equal to 2 cm is a good choice for giving the maximum possible ionization.

Density of Argon Metastable Atoms

In Fig. 6, the argon metastable atom density profile is illustrated for the cell with length and radius both equal to 2 cm. The metastable atom density reaches a pronounced maximum of about 10^{12} cm^{-3} in front of the cathode and a second, lower, maximum of about 10^{10} cm^{-3} at about 1.5 cm from the cathode. The overall density is, however, of the order of 1×10^9–5×10^9 cm^{-3}. An explanation for the occurrence of the two maxima was given elsewhere.[14] The corresponding density profiles calculated for the other cell dimensions are comparable. There is always a high maximum of about 10^{12} cm^{-3} close to the cathode, a steep drop behind this maximum and a second, less distinct, maximum near the anode end-wall. The only exception occurs in the case of a cell with length 0.5 cm and radius 2 cm: no second maximum was observed here, and the maximum in front of the cathode was broader and decreased more gradually towards the anode end-plate, as can be seen in Fig. 7. It appears from Fig. 7 that the overall density throughout the discharge cell is higher than for the cell with length and radius equal to 2 cm (Fig. 6). This trend is more or less continued on further increasing the cell length (*i.e.,* the overall density decreases slightly), although the effect is no longer so pronounced (at $l = 4$ cm the overall density beside the distinct maximum is about 1×10^9–2×10^9 cm^{-3}). The trend is also, to some extent, found on increasing the cell radius, *i.e.,* at $r = 0.5$ cm the overall density ranges from 5×10^9 to 5×10^{10} cm^{-3}, whereas at $r = 4$ cm the corresponding value is about 1×10^9–5×10^9 cm^{-3}. Hence, in the small cells, the overall argon metastable atom density appears to be higher than that in the larger cells. This is at first sight unexpected, since the loss of metastable species due to diffusion and de-excitation at the walls becomes less important in the larger cells.

However, another loss process, *i.e.* electron collisional transfer to the nearby resonant levels, appears to become dominant

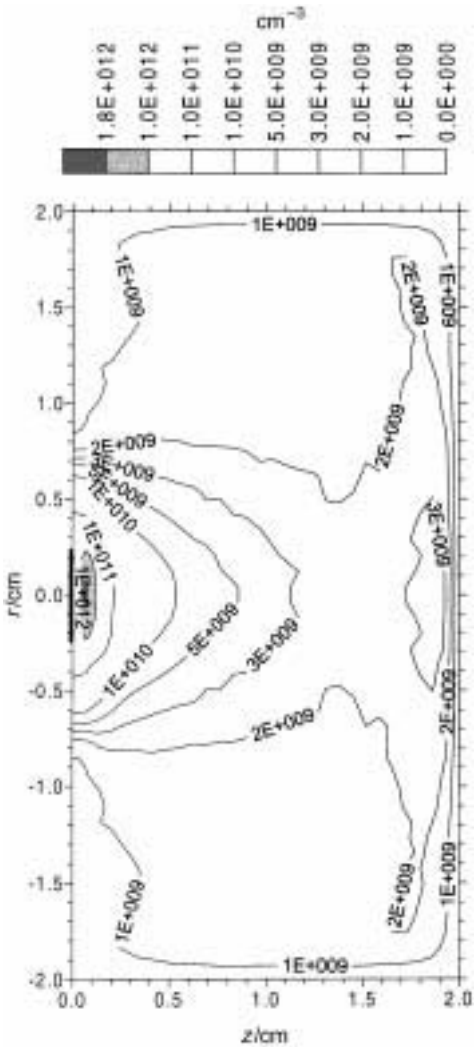

Fig. 6 Calculated density profile of the argon metastable atoms for the standard cell under the same discharge conditions as in Fig. 2.

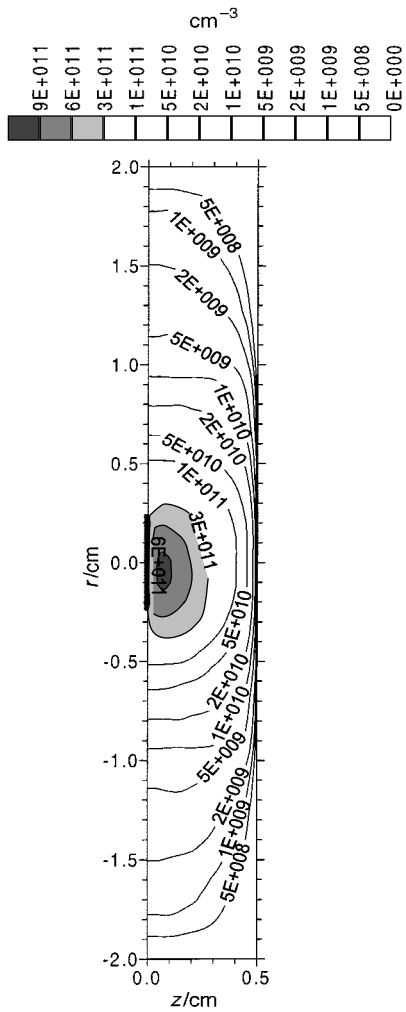

Fig. 7 Calculated density profile of the argon metastable atoms for the cell with $l=0.5$ cm and $r=2$ cm, at 1000 V, 1 Torr and 0.65 mA in an argon discharge with copper cathode.

in these larger cells, owing to the higher slow electron densities (see above). It was found that in the small cells, diffusion and de-excitation at the walls are more or less the dominant loss process for the argon metastable atoms (*i.e.* about 54% at $l=0.5$ and $r=2$ cm and about 41% at $l=2$ and $r=0.5$ cm, whereas the values for this loss process at $l=4$ and $r=2$ cm and at $l=2$ and $r=4$ cm are only about 5 and 20%, respectively), and in the larger cells electron collisional transfer to the nearby resonant levels is most important (*i.e.,* about 88 and 70% for $l=4$ and $r=2$ cm and $l=2$ and $r=4$ cm, respectively, compared with about 35 and 50% for $l=0.5$ and $r=2$ cm and $l=2$ and $r=0.5$ cm, respectively). The relative contributions of the other loss processes were found to be of minor importance and were comparable for all the cells investigated. The most important production process was in all cases electron impact excitation to the metastable levels although, especially in the small cells, argon ion and atom impact excitation were not negligible. For the cell of $l=0.5$ and $r=2$ cm, the importance of argon atom impact excitation was even found to be comparable to electron impact excitation. It should be mentioned, however, that these calculated data concerning the argon metastable atoms have to be considered with caution. The argon metastable atom density profile, calculated for a similar (so-called six-way cross) glow discharge cell, with comparable discharge conditions, was found not to be in complete agreement with results of laser induced fluorescence measurements,[14] which may indicate that the production and/or loss processes are not correctly described in the model, or that further processes would have to be incorporated. Nevertheless, the overall agreement with experiment was satisfactory, and therefore we believe that at least the trend observed in the present results will be correct.

Density of Sputtered Copper Atoms

Fig. 8 shows the sputtered copper atom density profile for the cell with $l=2$ and $r=2$ cm. The density is at its maximum close to the cathode and decreases towards the cell walls. This sputtered atom density profile, calculated for tantalum, for a comparable cell (six-way cross glow discharge cell) and discharge conditions, was in excellent agreement with results from laser induced fluorescence experiments,[13] which also supports the present results. The calculated sputtered copper atom density is clearly higher than that calculated for tantalum, since copper has a much higher sputtering yield than tantalum.[2] The copper atom density profiles, calculated for the other cell dimensions investigated, are similar to that in Fig. 8: a maximum is always reached at about 0.05–0.1 cm from the cathode, whereafter the density decreases towards the cell walls. Table 2 presents the maximum values for the different cell dimensions studied. The density appears to increase for lengths and radii between 0.5 and 2 cm, but remains constant on further increasing the dimensions. This indicates again that the effect of the cell walls is only important in the small cells, and that the cell with both length and radius equal to 2 cm is large enough to give high concentrations of sputtered atoms in the discharge.

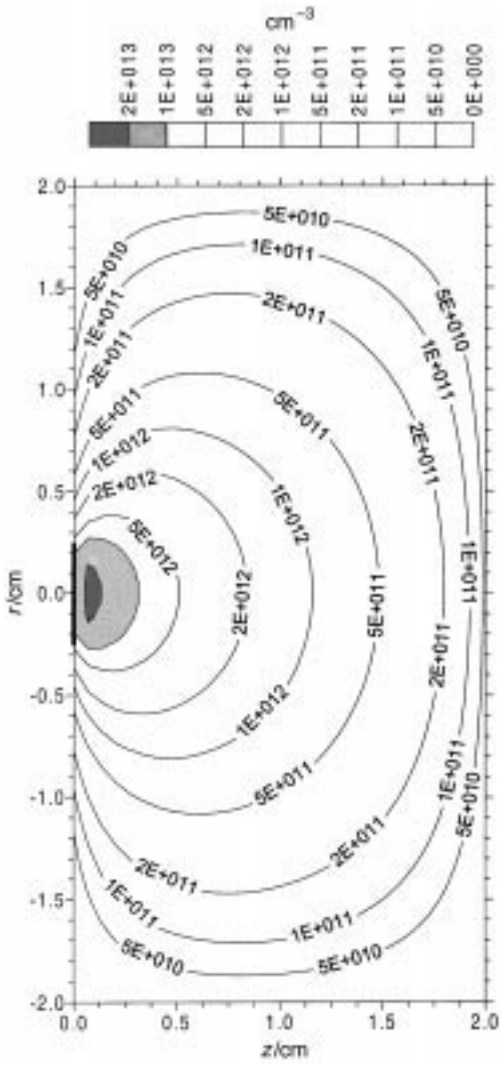

Fig. 8 Calculated density profile of the sputtered copper atoms for the standard cell under the same discharge conditions as in Fig. 2.

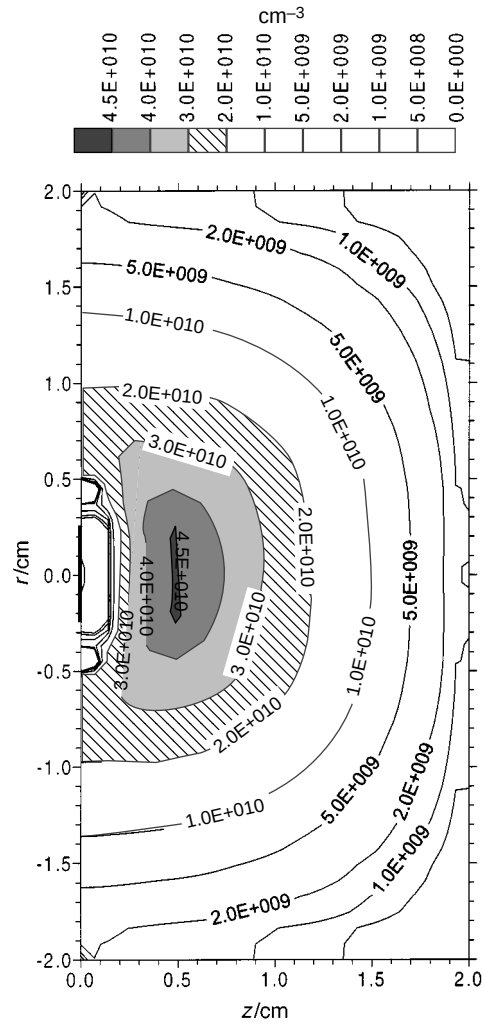

Fig. 9 Calculated density profile of the copper ions for the standard cell under the same discharge conditions as in Fig. 2.

Density and Flux of Copper Ions

The corresponding copper ion density distribution for the cell with $l=r=2$ cm is illustrated in Fig. 9. The density is low and approximately constant in the CDS, shows a steep increase at the CDS–NG interface, reaches a maximum at about 0.5 cm and decreases again to low values at the cell walls. The corresponding density profile of tantalum ions, calculated for a similar cell and discharge conditions, was, at least qualitatively, in good agreement with experimental results obtained by laser induced fluorescence spectrometry,[13] which supports the present results. The density profiles calculated for the other cell dimensions are qualitatively the same, *i.e.,* low values in the CDS and a maximum at about 0.5 cm from the cathode. The maximum values of the profiles are presented in Table 2. It appears that the copper ion density clearly increases for the dimensions from 0.5 to 2 cm, but it does not increase significantly for the larger cells.

The copper ion density profile is characterized by the same shape as the argon ion density profile (see Fig. 3), but it is nearly two orders of magnitude lower. The calculated ratios of copper ion to argon ion densities are also given in Table 2. These values also apply more or less to the ratios of copper ion to argon ion currents, both at the cathode and at the anode end-plate. When the glow discharge cell is used as an ion source for mass spectrometry (GDMS), the exit slit to the mass spectrometer is mostly situated at the anode end-plate. Therefore, if we assume that the transmission of ions through a double-focusing mass spectrometer is mass independent,[17] the ratio of currents at the anode end-plate can be seen as an estimate to the ratio of copper (matrix) ion peak to argon ion peak in the mass spectrum. Matrix to argon ion peak ratios of a few per cent are, indeed, often encountered in GDMS. Again, on increasing the cell dimensions from 0.5 up to 2 cm, it can be concluded that both the intensity of the copper ion peak in the mass spectrum and its ratio compared with the argon peak increase, and that hence better analytical sensitivity is expected. For cells with dimensions $\geqslant 2$ cm, however, there seems to be no further gain in sensitivity.

Ionization of Copper

Table 2 presents also the calculated ionization degrees of copper (*i.e.,* the ratio of the copper ion to copper atom densities, integrated over the total discharge region) for the different cell dimensions investigated. The ionization degree also appears to increase when the cell becomes larger. The effect is most pronounced for small cells (dimensions $\leqslant 2$ cm), and it is only weak for larger cells. The reason for this greater ionization seems to be attributable to the increasing role of asymmetric charge transfer for the ionization of copper, which is due to the higher argon ion densities in larger cells. The relative contributions of the three ionization processes for the sputtered copper atoms, for the different cell dimensions investigated, are illustrated in Fig. 10, and it appears that the

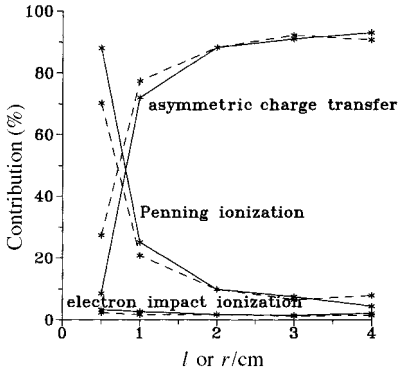

Fig. 10 Calculated relative contributions of asymmetric charge transfer, Penning ionization and electron impact ionization to the ionization of the sputtered copper atoms as a function of the cell dimensions at 1000 V and 1 Torr (argon discharge with copper cathode). The influence of the length (l) is given by the full lines and that of the cell radius (r) by the dashed lines.

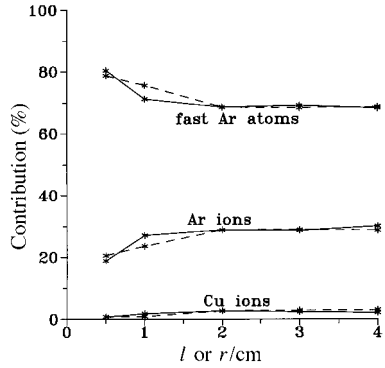

Fig. 12 Calculated relative contributions of the fast argon atoms, argon ions and copper ions to the sputtering process at the cathode as a function of the cell dimensions at 1000 V and 1 Torr (argon discharge with copper cathode). The influence of the length (l) is given by the full lines and that of the cell radius (r) by the dashed lines.

role of asymmetric charge transfer becomes increasingly important for larger cells. It seems to be the dominant process for all cell dimensions investigated, except for the two smallest cells ($l=0.5$ or $r=0.5$ cm), where Penning ionization is calculated to be the most significant process. The argon metastable atom density was found to be relatively higher in the small cells than in the larger cells (see above). Electron impact ionization appears to be of minor importance in all cases. It should be noted that the exact contributions of these three processes have to be considered with caution, since the rate coefficients for Penning ionization, and especially for asymmetric charge transfer, are not well known in the literature, and the values used (see ref. 11) are, therefore, subject to considerable uncertainties. Nevertheless, the general trend is expected to be correctly predicted.

Ionization of Argon

Whereas for the sputtered copper atoms asymmetric charge transfer and also Penning ionization are more important than electron impact ionization, the situation is completely different for the ionization of argon. Indeed, asymmetric charge transfer by argon ions and Penning ionization by argon metastables play, of course, no role in the ionization of argon, and electron impact ionization is the dominant process. Two other processes, *i.e.,* argon ion and atom impact ionization, come into play, however. Since these ionization mechanisms are only important in the CDS, close to the cathode, their final contributions are not dominant, but these processes are nevertheless not negligible.[5] In Fig. 11, the relative contributions of the ionization mechanisms for argon are depicted for the different cell dimensions under study. Electron impact ionization in the NG was found to be clearly dominant for all cases, but, since the NG shrinks accordingly when the cell dimensions decrease (and, moreover, the CDS becomes larger; see Table 2), the role of electron impact ionization in the CDS, and also of argon atom and ion impact ionization, becomes slightly more significant in the smaller cells.

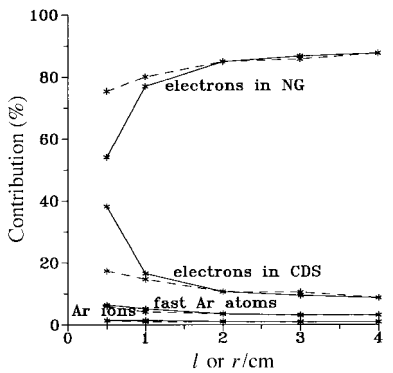

Fig. 11 Calculated relative contributions of electron impact ionization in the NG and in the CDS and of fast argon atom and argon ion impact ionization to the ionization of the argon atoms as a function of the cell dimensions at 1000 V and 1 Torr (argon discharge with copper cathode). The influence of the length (l) is given by the full lines and that of the cell radius (r) by the dashed lines.

Sputtering at the Cathode

Finally, since the ratio of copper ion flux to argon ion flux at the cathode increases when the cell becomes larger for cells with dimensions $\leqslant 2$ cm, the relative contribution of copper ions to the cathode sputtering (*i.e.,* self-sputtering) is also expected to rise. The relative contributions of copper ions, argon ions and fast argon atoms to sputtering are illustrated in Fig. 12 for the different cell dimensions studied. The role of the fast argon atoms appears to be dominant in all cases; the argon ions take second place and the copper ions contribute only a few percent. However, it can be noted that their role increases slightly when the cell dimensions change from 0.5 cm (*i.e.,* about 0.75%) to 2 cm (*i.e.,* about 2.5–3%). On further increasing the cell dimensions, the relative contributions of the copper ions, argon ions and fast atoms remain more or less constant.

CONCLUSION

A number of three-dimensional models, developed for a direct current glow discharge in argon, have been applied to different cells with lengths and radii varying from 0.5 to 4 cm to investigate the influence of the cell dimensions on the typical quantities calculated by the models, *e.g.*, the electric current as a function of voltage and pressure, the potential distributions and electric fields in the discharge and the densities of the plasma species. Special emphasis is placed on the use of the glow discharge as an ion source for mass spectrometry (GDMS) (*i.e.,* calculation of the importance of different ionization processes and the role of the sputtered atoms and ions in the discharge), but the results of the present investigation can also be extended to other applications of glow discharges.

It was found that the calculated results are qualitatively the same for the different cell dimensions investigated, but the absolute values are affected. The most important results are the following: on increasing the cell dimensions from 0.5 to 2 cm, the electric current at the same voltage and pressure

increases slightly, and the same applies to the densities of the plasma species. Moreover, the ionization degree of copper increases and the copper ion peak (and hence the peaks of the sputtered analyte ions in general) in the mass spectrum is predicted to be higher, yielding a better analytical sensitivity. On further increasing the cell dimensions to 4 cm, the calculated results remain more or less the same. The main reason is that, under the present discharge conditions, the range of the fast electrons for producing ionization collisions seems to be more or less limited to about 2 cm, and hence increasing the cell dimensions does not give rise to a higher degree of ionization, more electron multiplication and a higher plasma density. Consequently, also the ionization of copper, the copper ion density and the predicted analyte peaks in the mass spectrum no longer increase, and a further gain in analytical sensitivity is not expected. Therefore, under the present discharge conditions of 1000 V, 1 Torr and about 2 mA, it is expected that a glow discharge cell with length and radius both equal to 2 cm would yield the best analytical performance.

We have demonstrated that the modeling network is able to study the influence of cell dimensions on different plasma quantities. The models can, in principle, also be applied to specific cell geometries, and they can therefore be useful when developing new cells, for predicting trends in the plasma conditions and in the application results.

A. Bogaerts is financially supported by the Flemish Foundation for Scientific Research (FWO). The authors also acknowledge financial support from the Federal Services for Scientific, Technical and Cultural Affairs (DWTC/SSTC) of the Prime Minister's Office through IUAP-III (Conv. 49).

REFERENCES

1 Marcus, R. K., *Glow Discharge Spectroscopies*, Plenum Press, New York, 1993.
2 Chapman, B., *Glow Discharge Processes*, Wiley, New York, 1980.
3 Bogaerts, A., van Straaten, M., and Gijbels, R., *Spectrochim. Acta, Part B*, 1995, **50**, 179.
4 Bogaerts, A., Gijbels, R., and Goedheer, W. J., *J. Appl. Phys.*, 1995, **78**, 2233.
5 Bogaerts, A., and Gijbels, R., *J. Appl. Phys.*, 1995, **78**, 6427.
6 Bogaerts, A., and Gijbels, R., *Phys. Rev. A*, 1995, **52**, 3743.
7 Bogaerts, A., and Gijbels, R., *J. Appl. Phys.*, 1996, **79**, 1279.
8 Bogaerts, A., and Gijbels, R., *Fresenius' J. Anal. Chem.*, 1996, **355**, 853.
9 Bogaerts, A., Gijbels, R., and Goedheer, W. J., *Anal. Chem.*, 1996, **68**, 2296.
10 Bogaerts, A., van Straaten, M., and Gijbels, R., *J. Appl. Phys.*, 1995, **77**, 1868.
11 Bogaerts, A., and Gijbels, R., *Anal. Chem.*, 1996, **68**, 2676.
12 Bogaerts, A., *PhD Dissertation*, University of Antwerp, 1996.
13 Bogaerts, A., Wagner, E., Smith, B. W., Winefordner, J. D., Pollmann, D., Harrison, W. W., and Gijbels, R., *Spectrochim. Acta, Part B*, 1997, **52**, 205.
14 Bogaerts, A., Guenard, R. D., Smith, B. W., Winefordner, J. D., Harrison, W. W., and Gijbels, R., *Spectrochim. Acta, Part B*, 1997, **52**, 219.
15 Bogaerts, A., and Gijbels, R., *Spectrochim. Acta, Part B*, in the press.
16 van Straaten, M., Gijbels, R., and Vertes, A., *Anal. Chem.*, 1992, **64**, 1855.
17 Vieth, W., Huneke, J. C., *Spectrochim. Acta, Part B*, 1991, **46**, 137.

Paper 6/08262I
Received December 9, 1996
Accepted February 28, 1997